Ab initio study of the Coulomb interaction in Nb_xCo clusters: Strong on-site versus weak nonlocal screening

L. Peters,[1,*] E. Şaşıoğlu,[2,†] I. Mertig,[2] and M. I. Katsnelson[1]
[1]*Institute for Molecules and Materials, Radboud University Nijmegen, NL-6525 AJ Nijmegen, The Netherlands*
[2]*Institut für Physik, Martin-Luther-Universität Halle-Wittenberg, 06120 Halle (Saale), Germany*

(Received 19 September 2017; revised manuscript received 29 November 2017; published 16 January 2018)

By means of *ab initio* calculations in conjunction with the random-phase approximation (RPA) within the full-potential linearized augmented plane wave method, we study the screening of the Coulomb interaction in Nb_xCo ($1 \leqslant x \leqslant 9$) clusters. In addition, these results are compared with pure bcc Nb bulk. We find that for all clusters the on-site Coulomb interaction in RPA is strongly screened, whereas the intersite nonlocal Coulomb interaction is weakly screened and for some clusters it is unscreened or even antiscreened. This is in strong contrast with pure Nb bulk, where the intersite Coulomb interaction is almost completely screened. Furthermore, constrained RPA calculations reveal that the contribution of the Co $3d \rightarrow 3d$ channel to the total screening of the Co $3d$ electrons is small. Moreover, we find that both the on-site and intersite Coulomb interaction parameters decrease in a reasonable approximation linearly with the cluster size and for clusters having more than 20 Nb atoms a transition from 0D to 3D screening is expected to take place.

DOI: 10.1103/PhysRevB.97.045121

I. INTRODUCTION

The interest in the field of clusters is growing due to the increasing demand for nanotechnology. Besides the relevance for technology, clusters are also fundamentally very interesting. They behave in general very different from their bulk counterpart. Also their electronic and magnetic properties can drastically change by just adding or removing one atom [1–4]. For example, in a recent work on Nb_xCo clusters it is demonstrated that Nb_5Co and Nb_7Co are nonmagnetic, while Nb_4Co and Nb_6Co are strongly magnetic [5]. The physical origin of this behavior can be traced back to the drastic change of the electronic structure as a function of cluster size.

The study of bimetallic clusters offers a broader playground than for pure clusters. This has resulted in a number of intriguing observations [5–10]. For example, from an anion photoelectron spectroscopy study on bimetallic Nb_xCo clusters, it was observed that for $x = 6$ due to the addition of one Co atom to the Nb_x host, the electronic structure resembles that of a typical bulk semiconductor [8]. Therefore, this cluster was then proposed as a candidate for semiconductor materials.

From the theoretical side the bond properties and electronic structure of $(NbCo)_x$ clusters has been investigated by means of relativistic density functional theory (DFT) [11]. Furthermore, the geometry, stability, and electronic properties of neutral and anionic Nb_xCo clusters is compared with pure Nb_x clusters within a DFT study [12]. Recently a combined theoretical and experimental investigation has been performed on Nb_xCo clusters [5]. In this work the geometry is obtained from a comparison of experimentally and theoretically obtained vibrational spectra. With the geometry established the electronic structure is investigated in order to explain the magnetic properties obtained from magnetic deflection experiments.

To our knowledge a systematic assessment of screening and correlation effects in Nb_xCo clusters does not exist. This information is crucial in order to obtain a proper fundamental understanding of the system. Namely, correlation effects among the electrons inhibit in general an exact solution. Therefore, approximate methods are required in practice. The choice of a suitable approximate method requires knowledge of the effective Coulomb interaction in the system. More precisely, the gradient of the effective Coulomb interaction is of importance [13,14]. A very small gradient means that the effective Coulomb interaction is merely constant, while a very large gradient indicates a purely local effective Coulomb interaction. In the former case a mean-field treatment, i.e., single-particle approach, is probably a good choice, while for the latter it might be the (generalized) Hubbard model.

The aim of the present work is the *ab initio* determination of the Coulomb interaction for NbCo to Nb_7Co and Nb_9Co clusters. Besides being fundamentally interesting, such information is crucial to select an adequate theoretical method for a further investigation of the system. The geometries of Nb_3Co to Nb_7Co and Nb_9Co are well established from a comparison of theoretically and experimentally obtained vibrational spectra [5]. In addition, NbCo and Nb_2Co are considered, since the number of isomers is very small. All these clusters are known to be magnetic except Nb_5Co and Nb_7Co, which are nonmagnetic. By employing the full-potential linearized augmented plane wave (FLAPW) method using Wannier functions in conjunction with the random-phase approximation (RPA) [15–17], it is found that in these clusters the on-site Coulomb interaction in RPA is well screened, while the intersite Coulomb interactions are barely screened. Interestingly for NbCo the intersite interaction is unscreened, while for Nb_4Co even antiscreening occurs. The important

*L.Peters@science.ru.nl
†ersoy.sasioglu@physik.uni-halle.de

consequence being that the screened Coulomb interaction is almost constant throughout the clusters. For completeness these results are compared with pure Nb bulk for which only the on-site Coulomb interaction is appreciable, while the intersite Coulomb interactions are almost completely screened. Moreover, our constrained RPA calculations reveal that the Co $3d \rightarrow 3d$ channel only plays a minor role in the screening of the on-site Coulomb interaction of the Co $3d$ electrons. Finally, we find that both the on-site and intersite Coulomb interaction parameters decrease in a reasonable approximation linearly with the cluster size and for clusters having more than 20 Nb atoms a transition from 0D to 3D screening is expected to take place. The rest of the paper is organized as follows. The method and computational details are presented in Sec. II. Section III deals with the results and discussion and finally in Sec. IV we give the conclusions.

TABLE I. The bare, partially screened without the Co $3d \rightarrow 3d$ channel (cRPA) and fully screened (RPA) average on-site Coulomb interaction parameters for the Co $3d$ orbitals of the NbCo-Nb_7Co and Nb_9Co clusters obtained from *ab initio* calculations.

Cluster	Bare (eV)	cRPA (eV)	RPA (eV)
NbCo	22.2	7.9	7.7
Nb_2Co	22.2	5.9	5.8
Nb_3Co	22.3	5.6	5.5
Nb_4Co	22.6	5.2	5.0
Nb_5Co	22.7	4.7	4.6
Nb_6Co	22.7	4.4	4.3
Nb_7Co	22.7	4.1	4.1
Nb_9Co	22.9	3.9	3.8

II. METHOD AND COMPUTATIONAL DETAILS

In this work the screening of the Coulomb interaction in Nb_xCo clusters is calculated by means of the *ab initio* random phase approximation (RPA) method. The noninteracting reference system required for this method comes from a preceding DFT calculation. In the following we shortly explain the RPA method and for details we refer to Ref. [6]. The screened Coulomb interaction is defined as

$$W(\boldsymbol{r},\boldsymbol{r}',\omega) = \int d\boldsymbol{r}''\epsilon^{-1}(\boldsymbol{r},\boldsymbol{r}'',\omega)v(\boldsymbol{r}'',\boldsymbol{r}'), \tag{1}$$

where $\epsilon(\boldsymbol{r},\boldsymbol{r}'',\omega)$ is the dielectric function and $v(\boldsymbol{r}'',\boldsymbol{r}')$ is the bare Coulomb interaction potential. Since an exact expression for the dielectric function is not accessible, an approximation is required. In the RPA the dielectric function is approximated by

$$\epsilon(\boldsymbol{r},\boldsymbol{r}',\omega) = \delta(\boldsymbol{r}-\boldsymbol{r}') - \int d\boldsymbol{r}''v(\boldsymbol{r},\boldsymbol{r}'')P(\boldsymbol{r}'',\boldsymbol{r}',\omega), \tag{2}$$

where the polarization function $P(\boldsymbol{r}'',\boldsymbol{r}',\omega)$ is given by

$$P(\boldsymbol{r},\boldsymbol{r}',\omega) = \sum_{\sigma}\sum_{\boldsymbol{k},m}^{\text{occ}}\sum_{\boldsymbol{k}',m'}^{\text{unocc}} \varphi^{\sigma}_{\boldsymbol{k}m}(\boldsymbol{r})\varphi^{\sigma *}_{\boldsymbol{k}'m'}(\boldsymbol{r})\varphi^{\sigma *}_{\boldsymbol{k}m}(\boldsymbol{r}')\varphi^{\sigma}_{\boldsymbol{k}'m'}(\boldsymbol{r}') \times\left[\frac{1}{\omega-\Delta^{\sigma}_{\boldsymbol{k}m,\boldsymbol{k}'m'}} - \frac{1}{\omega+\Delta^{\sigma}_{\boldsymbol{k}m,\boldsymbol{k}'m'}}\right]. \tag{3}$$

Here $\Delta^{\sigma}_{\boldsymbol{k}m,\boldsymbol{k}'m'} = \epsilon^{\sigma}_{\boldsymbol{k}'m'} - \epsilon^{\sigma}_{\boldsymbol{k}m} - i\eta$ with $\epsilon^{\sigma}_{\boldsymbol{k}m}$ the single particle Kohn-Sham eigenvalues obtained from DFT and η a positive infinitesimal. Furthermore, the $\varphi^{\sigma}_{\boldsymbol{k}m}(\boldsymbol{r})$ are the single particle Kohn-Sham eigenstates with spin σ, wave number $\boldsymbol{k}$, and band index m. The tags occ and unocc above the summation symbol indicate that the summation is, respectively, over occupied and unoccupied states only.

Equations (1)–(3) constitute what is called the RPA of the dynamically screened Coulomb interaction. It is also possible to exclude certain screening contributions from Eq. (3), which is referred to as *constrained* RPA (cRPA). In this work the screening of the Coulomb interaction for the Co $3d$ electrons and Nb $4d$ electrons are investigated. One could for example exclude the screening contribution coming from the Co $3d$ states to obtain insight in their contribution to the total screening. More details on the method used in this work to exclude certain screening contributions can be found in Ref. [17]. Note that recently cRPA has become a very popular method to calculate Coulomb interaction parameters for different classes of materials [18–24].

The DFT calculations, providing the input of Eq. (3), are performed with the FLEUR code. This code is based on a FLAPW implementation [25]. All calculations are performed with an exchange-correlation functional in the generalized gradient approximation (GGA) as formulated by Perdew, Burke, and Ernzerhof (PBE) [26]. Furthermore, all calculations are without spin-orbit coupling. As will be demonstrated, the effect of screening is on the eV energy scale, while for the Co $3d$ and Nb $4d$ electrons the spin-orbit coupling strength is at least an order of magnitude smaller. In addition it will be shown (Table I and Fig. 3) that the contribution of these electrons to the screening is small with respect to the other electrons, the Co $4sp$ and Nb $5sp$ electrons. For such extended states the spin-orbit coupling strength is even smaller than for the Co $3d$ and Nb $4d$ electrons. Therefore, spin-orbit coupling effects are expected to be small for the consideration of effective interactions. Since FLEUR is a **k**-space code, a supercell approach was employed for the cluster calculations, with a large vacuum between clusters that were repeated in a periodic lattice. In order to prevent the interaction between clusters of different unit cells we performed tests for different unit cell sizes. We found that for a large unit cell of 12 Å dimensions the results are converged to within a few percent. Therefore, this unit cell size is used for our calculations. Furthermore, for the cluster calculations the cutoff for the plane waves is 4.0 bohr^{-1}, $l_{\text{cut}} = 8$, and the Γ point is the only **k** point considered. For the calculations of bulk bcc Nb we use the same parameters with a $20 \times 20 \times 20$ **k**-point mesh and experimental lattice parameter of 3.3 Å of the bcc lattice. The ground state geometric and magnetic structure of the Nb_3Co to Nb_7Co and Nb_9Co clusters is obtained from Ref. [5] (see also Fig. 1). More precisely, the geometries and magnetic structure are obtained from a comparison of calculated and measured vibrational spectra. Structures of NbCo, Nb_2Co, and Nb_8Co were not addressed in Ref. [5]. Since the structure for Nb_8Co is unclear due to the many possible isomers, we will only address NbCo and Nb_2Co in addition. In order to obtain the ground state geometry of NbCo and Nb_2Co we performed the ATK-DFT

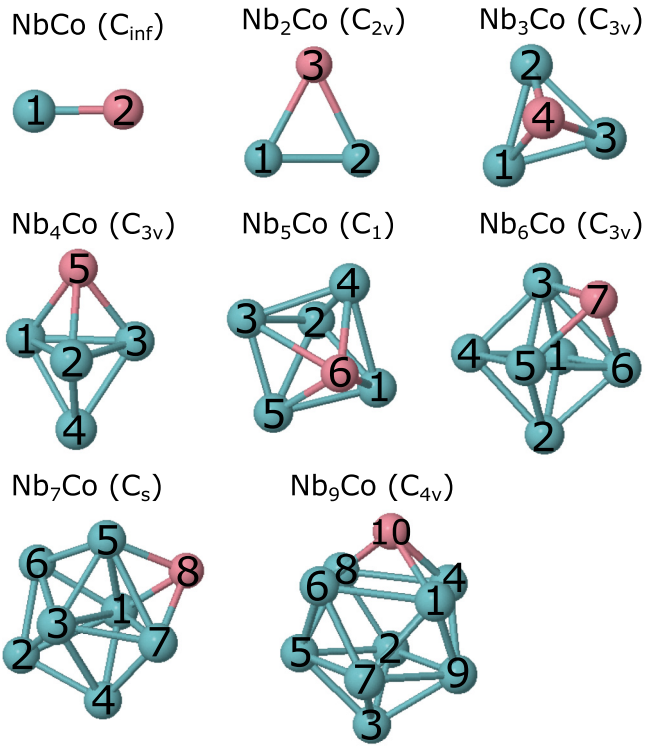

FIG. 1. The geometry of the NbCo to Nb_7Co and Nb_9Co clusters. Between brackets the point symmetry group of the cluster is indicated. The blue spheres correspond to the Nb atoms and the red spheres to the Co atoms.

calculations [27] using the GGA-PBE exchange-correlation functional [26] and the SG15-medium combination of norm-conserving pseudopotentials and LCAO basis sets [28,29]. The total energy and forces have been converged at least to 10^{-4} eV and 0.01 eV/Å, respectively.

The DFT calculations are used as an input for the SPEX code to perform RPA and cRPA calculations for the screened and partially screened (Hubbard U) Coulomb interaction [30]. The SPEX code uses the Wannier90 library to construct the maximally localized Wannier functions [31,32]. For this construction we used per spin channel six states per Co atom, i.e., five $3d$ states and one $4s$ state, and nine states per Nb atom, five $4d$ states, one $5s$ state, and three $5p$ states. More precisely, the maximally localized Wannier functions are used to project the screened (bare) Coulomb interaction of Eq. (1) on

$$U^{\sigma_1,\sigma_2}_{in_1,jn_3,in_2,jn_4}(\omega) = \iint d\boldsymbol{r}d\boldsymbol{r}' w^{\sigma_1 *}_{in_1}(\boldsymbol{r}) w^{\sigma_2 *}_{jn_3}(\boldsymbol{r}') W(\boldsymbol{r},\boldsymbol{r}',\omega) w^{\sigma_2}_{jn_4}(\boldsymbol{r}') w^{\sigma_1}_{in_2}(\boldsymbol{r}). \quad (4)$$

Here $w^{\sigma}_{in}(\boldsymbol{r})$ is a maximally localized Wannier function located at site i and spin σ. In this work we only consider the static limit ($\omega = 0$). Furthermore, we use Slater parametrization,

$$U_i = \frac{1}{(2l+1)^2} \sum_{m,m'} U^{\sigma_1,\sigma_2}_{im,im',im,im'}(\omega = 0)$$

and

$$V_{ij} = \frac{1}{(2l+1)^2} \sum_{m,m'} U^{\sigma_1,\sigma_2}_{im,jm',im,jm'}(\omega = 0). \quad (5)$$

Here U_i is the screened (bare) on-site Coulomb interaction at site i and V_{ij} is the screened (bare) intersite Coulomb interaction between sites i and j. Note that although the matrix elements of the Coulomb potential are formally spin dependent due to the spin dependence of the Wannier functions, we find that this dependence is negligible in practice.

III. RESULTS AND DISCUSSION

In Fig. 1 the geometry of the NbCo to Nb_7Co and Nb_9Co clusters is depicted. The blue spheres correspond to the Nb atoms and the red spheres to the Co atoms. Between brackets the point symmetry group of the clusters is indicated. In the following we first address the fully screened (RPA) and partially screened without the Co $3d \rightarrow 3d$ channel (cRPA) on-site Coulomb interaction matrix elements of the Co $3d$ electrons for the Nb_xCo clusters. This provides insight into the contribution of the Co $3d \rightarrow 3d$ channel to the total screening process. Second, the fully screened on-site and intersite Coulomb interaction matrix elements of the Nb $4d$ and Co $3d$ orbitals are investigated. Finally, we make a comparison with pure bcc Nb bulk and investigate the influence of the Nb $4d \rightarrow 4d$ channel on the screening of the on-site and intersite Coulomb interaction of the Nb $4d$ electrons. Note that the partially screened on-site Coulomb interaction is usually referred to as Hubbard U and is what enters effective models, e.g., the Hubbard model.

In Table I the bare, partially screened without the Co $3d \rightarrow 3d$ channel (cRPA) and fully screened (RPA) average on-site Coulomb interaction matrix elements of the Co $3d$ electrons are presented. As it is seen the bare interaction is constant as a function of cluster size, while the partially and fully screened interactions decrease with size. This can be attributed to the increase of screening channels with increasing cluster size rather than the delocalization of the Wannier functions. Note that very similar matrix elements for the on-site bare Coulomb interaction for all clusters reflect the fact that the localization of the Wannier functions does not change with increasing the cluster size. Furthermore, the obtained cRPA and RPA Coulomb matrix elements for the Co $3d$ orbitals are very close to each other, which means that the contribution of the Co $3d \rightarrow 3d$ channel to the total screening is very small compared to the other screening channels (see Table I).

In Tables II and III the bare (fourth column) and fully screened (fifth column) on-site and intersite average Coulomb interaction parameters for Nb $4d$ and Co $3d$ orbitals are presented for the Nb_xCo clusters. Due to the symmetry of some clusters (see Fig. 1), some Nb atoms are equivalent. In Fig. 1 for Nb_2Co atoms 1 and 2 are equivalent, for Nb_3Co 1, 2, and 3 are equivalent, for Nb_4Co 1, 2, and 3 are equivalent, for Nb_5Co there are no equivalent atoms, for Nb_6Co 3, 5, and 6, and 1, 2, and 4 are equivalent, for Nb_7Co 5 and 7, and 4 and 6 are equivalent, and for Nb_9Co 1, 4, 6, and 8, and 2, 5, 7, and 9 are equivalent. In Tables II and III only symmetry unequivalent interactions are shown. Furthermore, in the first column U_1 corresponds to the on-site Coulomb interaction of atom 1 and $V_{1,2}$ to the intersite Coulomb interaction between atoms 1 and 2 (see Fig. 1). The second column indicates between what type of atoms this refers and the third column corresponds to the distance in Å between them. From this table

TABLE II. The bare and fully screened (RPA) average Coulomb interaction parameters for the Nb 4*d* and Co 3*d* orbitals for the NbCo to Nb_5Co obtained from *ab initio* calculations. Here U_1 corresponds to the on-site Coulomb interaction of atom 1 and $V_{1,2}$ to the intersite Coulomb interaction between atoms 1 and 2 (see Fig. 1). The second column indicates between what type of atoms this refers and the third column corresponds to the distance in Å between them. Note that due the symmetry of some clusters, some Nb atoms are equivalent.

U/V	Atom	Distance (Å)	Bare (eV)	RPA (eV)
		NbCo		
U_1	Nb	0	11.2	7.2
U_2	Co	0	22.2	7.7
$V_{1,2}$	Nb-Co	1.99	7.0	7.0
		Nb_2Co		
U_1	Nb	0	10.0	5.2
U_3	Co	0	22.2	5.8
$V_{1,2}$	Nb-Nb	2.16	6.0	4.9
$V_{1,3}$	Nb-Co	2.33	6.1	5.0
		Nb_3Co		
U_1	Nb	0	10.7	5.0
U_4	Co	0	22.3	5.5
$V_{1,2}$	Nb-Nb	2.40	5.6	4.5
$V_{1,4}$	Nb-Co	2.47	5.7	4.6
		Nb_4Co		
U_1	Nb	0	11.0	4.6
U_4	Nb	0	10.8	4.5
U_5	Co	0	22.6	5.0
$V_{1,5}$	Nb-Co	2.40	6.0	4.2
$V_{1,4}$	Nb-Nb	2.52	5.5	4.1
$V_{1,2}$	Nb-Nb	2.61	5.4	4.1
$V_{4,5}$	Nb-Co	3.89	4.0	**4.1**
		Nb_5Co		
U_1	Nb	0	11.2	4.3
U_2	Nb	0	10.8	4.3
U_3	Nb	0	11.0	4.3
U_4	Nb	0	11.2	4.3
U_5	Nb	0	11.2	4.3
U_6	Co	0	22.7	4.6
$V_{1,6}$	Nb-Co	2.27	6.3	3.9
$V_{4,6}$	Nb-Co	2.28	6.2	3.8
$V_{5,6}$	Nb-Co	2.32	6.1	3.8
$V_{3,5}$	Nb-Nb	2.40	5.7	3.8
$V_{1,2}$	Nb-Nb	2.44	5.6	3.8
$V_{2,3}$	Nb-Nb	2.49	5.5	3.8
$V_{2,4}$	Nb-Nb	2.50	5.5	3.8
$V_{3,4}$	Nb-Nb	2.63	5.3	3.7
$V_{1,5}$	Nb-Nb	2.69	5.3	3.7
$V_{3,6}$	Nb-Co	2.81	5.1	3.8
$V_{1,4}$	Nb-Nb	2.92	4.9	3.7
$V_{2,5}$	Nb-Nb	2.99	4.8	3.7
$V_{2,6}$	Nb-Co	3.27	4.5	3.8
$V_{4,5}$	Nb-Nb	3.68	4.1	3.7
$V_{1,3}$	Nb-Nb	3.72	4.1	3.7

it can be seen that besides for the Co 3*d* electrons also for the Nb 4*d* electrons the on-site Coulomb interaction is well screened and decreases with cluster size. On the other hand, the intersite Coulomb interaction is much less screened and is more or less constant as a function of interatomic distance.

TABLE III. The same as Table II for Nb_6Co, Nb_7Co, and Nb_9Co clusters. Here U_1 corresponds to the on-site Coulomb interaction of atom 1 and $V_{1,2}$ to the intersite Coulomb interaction between atoms 1 and 2 (see Fig. 1 for the geometry of the corresponding clusters).

U/V	Atom	Distance (Å)	Bare (eV)	RPA (eV)
		Nb_6Co		
U_1	Nb	0	11.3	4.0
U_3	Nb	0	11.3	4.0
U_7	Co	0	22.7	4.3
$V_{3,7}$	Nb-Co	2.33	6.2	3.5
$V_{3,4}$	Nb-Nb	2.53	5.5	3.5
$V_{1,2}$	Nb-Nb	2.73	5.2	3.4
$V_{3,5}$	Nb-Nb	2.88	5.0	3.4
$V_{2,3}$	Nb-Nb	3.78	4.0	3.3
$V_{2,7}$	Nb-Co	3.91	3.9	3.4
		Nb_7Co		
U_1	Nb	0	11.3	3.9
U_2	Nb	0	11.2	3.9
U_3	Nb	0	11.2	3.9
U_4	Nb	0	11.3	3.9
U_5	Nb	0	11.4	3.9
U_8	Co	0	22.7	4.1
$V_{5,8}$	Nb-Co	2.30	6.2	3.4
$V_{1,8}$	Nb-Co	2.43	5.9	3.3
$V_{2,4}$	Nb-Nb	2.46	5.6	3.4
$V_{1,4}$	Nb-Nb	2.53	5.5	3.4
$V_{3,5}$	Nb-Nb	2.54	5.5	3.3
$V_{2,3}$	Nb-Nb	2.56	5.4	3.3
$V_{3,4}$	Nb-Nb	2.83	5.0	3.3
$V_{1,5}$	Nb-Nb	2.85	5.0	3.3
$V_{1,2}$	Nb-Nb	2.86	5.0	3.3
$V_{5,7}$	Nb-Nb	2.90	5.0	3.3
$V_{1,3}$	Nb-Nb	3.15	4.6	3.3
$V_{3,8}$	Nb-Co	3.78	4.1	3.3
$V_{4,8}$	Nb-Co	3.97	3.9	3.3
$V_{4,6}$	Nb-Nb	3.98	3.9	3.2
$V_{2,5}$	Nb-Nb	4.08	3.8	3.2
$V_{4,5}$	Nb-Nb	4.26	3.7	3.2
$V_{2,8}$	Nb-Co	4.88	3.4	3.3
		Nb_9Co		
U_1	Nb	0	11.5	3.4
U_2	Nb	0	11.4	3.5
U_3	Nb	0	11.4	3.4
U_{10}	Co	0	22.9	3.8
$V_{1,10}$	Nb-Co	2.42	6.0	3.0
$V_{1,7}$	Nb-Nb	2.53	5.5	2.9
$V_{2,3}$	Nb-Nb	2.57	5.5	2.9
$V_{1,4}$	Nb-Nb	2.82	5.1	2.9
$V_{2,5}$	Nb-Nb	2.87	5.0	2.9
$V_{2,10}$	Nb-Co	3.94	3.9	2.9
$V_{1,8}$	Nb-Nb	3.99	3.9	2.9
$V_{2,7}$	Nb-Nb	4.05	3.8	2.8
$V_{1,3}$	Nb-Nb	4.11	3.8	2.8
$V_{1,2}$	Nb-Nb	4.22	3.7	2.8
$V_{3,10}$	Nb-Co	4.96	3.3	2.9

This appears to be due to a decrease in the screening as a function of increasing interatomic distance. Interestingly for NbCo the intersite interaction is unscreened, while for Nb_4Co there is even antiscreening present between Nb and Co at

an interatomic distance of 3.89 Å. Antiscreening means that the screened interaction is larger than the bare interaction. By considering the effective interaction between two point charges in a medium, screening is understood to be due to the response (polarization) of the medium to these charges. Similarly antiscreening occurs when the medium is polarized in such a way to increase the bare interaction between the two point charges. This situation is known to occur only for low dimensional systems such as carbon nanotubes, nanoribbons, wires, molecules, and clusters [13,14]. From a simplistic point of view the two induced point charges can be considered as giving rise to point dipoles at the positions of the polarizable atoms that constitute the medium. Each point dipole produces an electric field and depending on its orientation it either increases or decreases the bare electric field coming from the two point charges. Roughly the point dipoles in between the two point charges are oriented to increase, antiscreen, the bare interaction, whereas the other surrounding point dipoles lead to a reduction, screening, of the bare interaction [14]. Therefore, the occurrence of antiscreening crucially depends on the dimensionality of the system and distance between the induced point charges. More precisely, for low dimensional systems the ratio of the region between the point charges and the rest of the medium is larger.

Antiscreening was also recently found in Fe_xO_y clusters by means of *ab initio* calculations [6]. However, the antiscreening appears to be more pronounced in Fe_xO_y clusters than in Nb_xCo clusters. In order to qualitatively understand this, the microscopic point-dipole model can be used. Within this model the atoms of the system are considered as classical polarizable point dipoles. These point dipoles are then allowed to respond to an external perturbation, e.g., induced point charges. From investigations on low dimensional systems by means of this microscopic point-dipole model, it is well established that antiscreening delicately depends on the geometry and polarizability of the atoms constituting the system [13,14]. However, in general it is demonstrated that the interatomic distance at which antiscreening occurs increases with increasing polarizability (see for example Fig. 1.10 of Ref. [14]). Furthermore, from for example *ab initio* calculations on isolated atoms it is known that the polarizability of Nb is larger than that of Fe, Co, and O [33]. Fe and Co have a similar polarizability, which is again larger than that of O. Based on these observations antiscreening in Nb_xCo clusters is expected to occur at larger interatomic distances compared to Fe_xO_y clusters, which explains why antiscreening is more pronounced in the latter.

The discussion above on the difference in antiscreening between Nb_xCo and Fe_xO_y clusters is based on the microscopic point-dipole model. It is however not clear if these clusters can be modeled by a collection of point dipoles. Therefore, it is instructive to also discuss antiscreening differences based on Eq. (3). It is known that antiscreening only occurs in low dimensional semiconductors and insulators [13,14,34,35]. As mentioned above, the critical distance for the appearance of antiscreening increases with increasing polarizability, which can be traced back to the distribution of the occupied and unoccupied electronic states around the Fermi energy (strictly speaking chemical potential for the clusters). In Fig. 2 we present the density of states for Fe_2O_3 and Nb_3Co clusters, which is calculated using the Gaussian method with

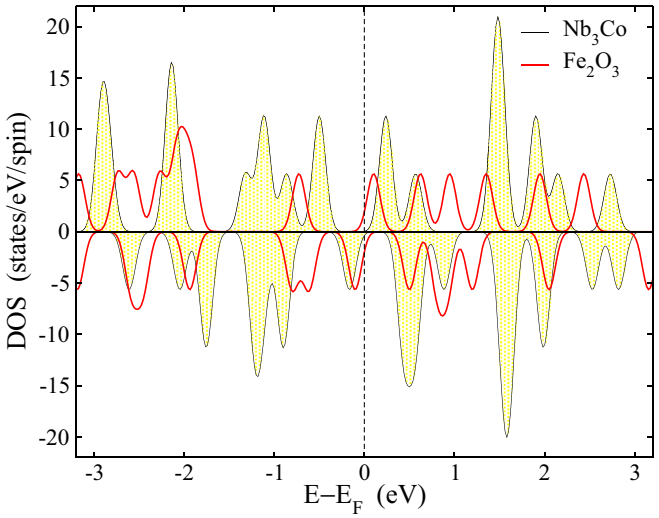

FIG. 2. Calculated spin-resolved total density of states for Fe_2O_3 and Nb_3Co clusters. The Fermi energy (chemical potential) is set to zero.

a broadening parameter of 0.1 eV. The polarizability [see Eq. (3)] is inversely proportional to the energy difference between occupied and unoccupied states, i.e., the smaller the energy difference the larger the polarizability. Indeed, as seen in Fig. 2, the Nb_3Co cluster has more states around the chemical potential with respect to the Fe_2O_3 cluster despite similar HOMO-LUMO energy gaps of both clusters. As a consequence, the contribution of the term between square brackets in Eq. (3) is larger for the Nb_3Co cluster giving rise to smaller Coulomb matrix elements and absence of antiscreening for intersite Coulomb interactions. Thus, similar as for the microscopic point-dipole model, a small polarization or equivalently polarizability of the system is required to observe antiscreening at short distances.

A similar discussion holds for all other clusters, for instance the NbCo cluster has a similar molecular energy level distribution around the chemical potential as Fe_3O_4 (not shown). Then, antiscreening is expected to occur at similar intersite distances in these clusters. For Fe_3O_4 this is expected to occur a bit below 3.4 Å (see Table I of Ref. [6]), while for NbCo indeed just above 3.0 Å. Furthermore, although Nb_2Co and Nb_3Co show a similar molecular energy spectrum around the chemical potential as the Fe_4O_6 cluster, antiscreening is not observed, because the intersite distances are too small compared to Fe_4O_6. For Nb_4Co and larger clusters the density of molecular energy levels around the chemical potential increases and is quite a bit denser than for the Fe_xO_y clusters. Therefore, antiscreening in these clusters is only expected for large intersite distances. For example, in Nb_4Co it occurs at 3.89 Å, while for Nb_7Co at an intersite Nb-Co distance of 4.88 Å the situation is very close to antiscreening.

It is instructive to compare the Nb_xCo results with pure Nb bulk. In Table IV the bare, partially screened (without the Nb $4d \rightarrow 4d$ channel), and fully screened on-site and intersite Coulomb interaction matrix elements of the Nb $4d$ electrons are presented. From this table it is clear that the intersite Coulomb interaction in RPA is almost completely screened.

TABLE IV. The bare, partially screened without the Nb $4d \rightarrow 4d$ channel (cRPA), and fully screened (RPA) average on-site and intersite Coulomb interaction parameters for the Nb $4d$ orbitals of pure Nb bulk. Here the first column refers to the distance in Å between two Nb atoms, i.e., zero corresponds to the on-site interaction.

Distance (Å)	Bare (eV)	cRPA (eV)	RPA (eV)
0	13.81	2.62	0.83
2.86	5.01	0.08	0.01
3.30	4.35	0.04	0.00
4.67	3.11	0.01	0.00
5.72	2.57	0.00	0.00

This is in contrast with what is observed for the clusters (Tables II and III). Furthermore, the fully screened on-site Coulomb interaction is more screened than for the clusters. The important observation for pure Nb bulk is that the effective Coulomb interaction is not constant throughout the system. Instead, it is localized, i.e., short ranged with a large gradient. Furthermore, the contribution of the Nb $4d \rightarrow 4d$ channel to the screening can be investigated from Table IV. Both for the on-site and intersite effective interaction this contribution is small, about 1.8 and 0.07 eV (for the nearest-neighbor interaction), compared to the contribution of about 11 and 4.9 eV of the other channels. The main screening contribution comes from the $5s$ states, which are present around the Fermi level.

For the Nb_xCo clusters the influence of the Nb $4d \rightarrow 4d$ channel can be obtained from an inspection of Fig. 3. Here an average of the partially screened (without the Nb $4d \rightarrow 4d$ channel) and fully screened on-site and nearest-neighbor

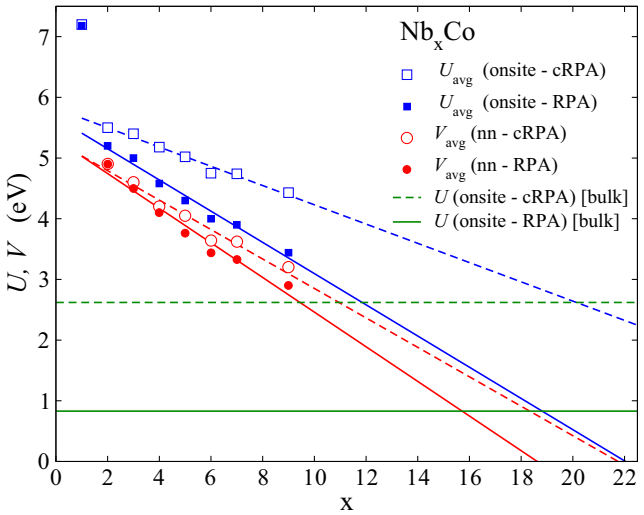

FIG. 3. The averaged partially screened without the Nb $4d \rightarrow 4d$ channel and fully screened on-site U_{avg} (on-site) and nearest-neighbor intersite V_{avg} (nn) matrix elements between Nb $4d$ electrons as a function of cluster size (x) for the Nb_xCo clusters. Here x corresponds to the number of Nb atoms in the Nb_xCo cluster. Ignoring the smallest cluster ($x = 1$), the blue and red solid and dashed lines represent an extrapolation of the data points. The green solid and dashed lines represent, respectively, the on-site fully screened and partially screened Coulomb interaction for pure Nb bulk.

intersite Coulomb interaction parameters for the Nb $4d$ orbitals are presented as a function of cluster size. The cluster size is indicated by x, which represents the number of Nb atoms in the Nb_xCo clusters. It appears that the contribution of the Nb $4d \rightarrow 4d$ channel to the screening of the on-site and intersite effective interaction increases with cluster size. For instance for the on-site interaction this contribution is about 0.3 eV for Nb_2Co and becomes about 0.9 eV for the Nb_9Co cluster. In case of the nearest-neighbor intersite interaction the contribution for Nb_2Co is almost 0 eV and becomes about 0.3 eV for Nb_9Co. Compared to the contributions of the other channels (see Tables II and III for the unscreened bare values), it can be concluded that the contribution of the Nb $4d \rightarrow 4d$ channel to the screening is small. Namely for the on-site interaction the contribution of the other channels is about 5 eV for Nb_2Co and becomes about 8 eV for Nb_9Co. In case of the nearest-neighbor intersite interaction this is about 1 eV for Nb_2Co and 2.5 eV for Nb_9Co.

It is interesting to obtain insight at what cluster size the behavior of the screened Coulomb interaction becomes bulklike. For this purpose Fig. 3 is used again, where the averaged on-site and nearest-neighbor intersite screened and partially screened Coulomb interaction parameters between Nb $4d$ electrons are presented as a function of cluster size and compared with the pure Nb bulk values of Table IV (green dashed and solid lines for the on-site cRPA and RPA interactions, respectively). The blue and red solid (dashed) lines correspond to a linear extrapolation of the Nb_xCo cluster data points for which the smallest cluster ($x = 1$) is ignored. From these extrapolations it appears that both the averaged on-site and intersite screened and partially screened Coulomb interaction depend in a reasonable approximation linearly on the cluster size. At a cluster size of $x = 20$ both the on-site and nearest-neighbor intersite screened (partially screened) interaction have reached their corresponding bulk values, i.e., 0.83 eV (2.62 eV) and 0.01 eV (0.08 eV), respectively. Therefore, we expect Nb_xCo clusters with x larger than 20 to have a bulklike behavior.

Finally, we would like to comment on the strength of the electronic correlations in the Nb_xCo clusters and Nb bulk. As shown in Tables II and III the effective Coulomb interaction is more or less constant throughout the clusters. In contrast for Nb bulk it has a strong gradient and is local in nature. Although the effective Coulomb interaction in Nb bulk is mainly local, it should not be considered as a (strongly) correlated material. For this purpose the bandwidth should also be taken into account. The bandwidth is about 7.5 eV [36], which is much larger than the effective on-site Coulomb interaction of 0.83 eV (see Table IV). Therefore, it should be interpreted as a weakly correlated material and standard DFT is expected to provide a good description of the essential physics. This is confirmed by DFT studies on the elastic properties, band structure, and electron-phonon coupling of Nb bulk, which are in good agreement with experiments [36–38]. Due to the almost constant effective Coulomb interaction in the Nb_xCo clusters, it is also expected that DFT should be able to capture the essential physics. This is confirmed by a comparison of the vibrational spectra obtained within DFT and experiments [5]. Furthermore, in Ref. [12] it is correctly predicted within DFT that Nb_7Co should be nonmagnetic. The

wrong prediction of Nb_5Co to be magnetic is probably due to the consideration of the wrong geometry (see Ref. [5]). Besides providing an explanation for the success of DFT in these clusters, our results are crucial to select an adequate method for future investigations on many-body effects, e.g., quasiparticle lifetimes. For example, intuitively one might expect DFT in combination with the dynamical mean-field theory (DMFT) [39] to be suitable for this purpose, because the Co atom can be interpreted as an impurity in a Nb_x host. Since DMFT only properly treats local correlations, while we have demonstrated nonlocal correlations to be also important, this is not a justified choice. Therefore, an extended Hubbard-like model or the consideration of the cluster within multiplet ligand-field theory [40] are probably more suitable choices.

In addition we expect that due to the almost constant effective interaction in the Nb_xCo clusters, the observed trends are robust with respect to the choice of the exchange-correlation functional. For example, the local density approximation (LDA) [41] and GGA are expected to perform similarly due to the constant interaction, because both methods are derived in the limit of a (nearly) uniform electron gas. As a test we made for all clusters a comparison between the density of states in GGA and LDA. Since they were found to be very similar around the Fermi level, it is indeed expected based on Eq. (3) that our results are robust with respect to the choice of the exchange-correlation functional.

IV. CONCLUSION

We have performed RPA and cRPA calculations to reveal the screening of the Coulomb interaction in Nb_xCo ($1 \leqslant x \leqslant 9$) clusters and pure Nb bulk. We have found that in both the clusters and the bulk the on-site Coulomb interaction in RPA is well screened. On the other hand, the intersite Coulomb interaction is much less screened in the clusters resulting in an almost constant interaction throughout the clusters. This is in contrast with pure Nb bulk, where the intersite Coulomb interaction in RPA is almost completely screened. Our cRPA calculations have shown that the contribution of the Co $3d \rightarrow 3d$ channel to the total screening process of the on-site Coulomb parameters of the Co $3d$ electrons is negligible. Furthermore, for the clusters investigated the contribution of the Nb $4d \rightarrow 4d$ channel to effective on-site and intersite Coulomb parameters of the Nb $4d$ electrons appears to be small compared to that of the total screening contribution. Based on our findings we expect both for the Nb_xCo clusters and Nb bulk that correlation effects play a minor role and that standard DFT is able to capture the essential physics. For the clusters this is due to the almost constant effective Coulomb interaction and for the bulk due to the bandwidth being much larger than the essentially local effective Coulomb interaction. Finally, it has been found that both the on-site and intersite Coulomb interaction parameters decrease in a reasonable approximation linearly with cluster size and for Nb_xCo clusters having more than 20 Nb atoms a transition from 0D to 3D screening is expected to take place.

ACKNOWLEDGMENTS

The Nederlandse Organisatie voor Wetenschappelijk Onderzoek (NWO) and SURFsara are acknowledged for the usage of the LISA supercomputer and their support. L.P. and M.I.K. acknowledges a support by European Research Council (ERC) Grant No. 338957. E.S. and I.M. greatly acknowledge the funding provided by the European Union (EFRE).

[1] F. Liu, S. N. Khanna, and P. Jena, Phys. Rev. B **43**, 8179 (1991).
[2] C. N. van Dijk, T. Rasing, A. Kirilyuk, J. Bowlan, A. Liang, and W. A. de Heer, J. Appl. Phys. **107**, 09B526 (2010).
[3] L. Peters, I. Di Marco, M. S. Litsarev, A. Delin, M. I. Katsnelson, A. Kirilyuk, B. Johansson, B. Sanyal, and O. Eriksson, Phys. Rev. B **92**, 035143 (2015).
[4] L. Peters, S. Ghosh, B. Sanyal, C. van Dijk, J. Bowlan, W. de Heer, A. Delin, I. Di Marco, O. Eriksson, M. I. Katsnelson, B. Johansson, and A. Kirilyuk, Sci. Rep. **6**, 19676 (2016).
[5] A. Diaz-Bachs, L. Peters, R. Logemann, V. Chernyy, J. M. Bakker, M. I. Katsnelson, and A. Kirilyuk, arXiv:1709.01534.
[6] L. Peters, E. Şaşıoğlu, S. Rossen, C. Friedrich, S. Blügel, and M. I. Katsnelson, Phys. Rev. B **95**, 155119 (2017).
[7] D. Dieleman, M. Tombers, L. Peters, J. Meyer, S. Peredkov, J. Jalink, M. Neeb, W. Eberhardt, T. Rasing, G. Niedner-Schatteburg, and A. Kirilyuk, Phys. Chem. Chem. Phys. **17**, 28372 (2015).
[8] A. Pramann, K. Koyasu, A. Nakjima, and K. Kaya, Int. J. Mass Spectrom. **229**, 77 (2003).
[9] A. Pramann, A. Nakajima, and K. Kaya, Chem. Phys. Lett. **347**, 366 (2001).
[10] T. G. Taylor, K. F. Willey, M. B. Bishop, and M. A. Duncan, J. Phys. Chem. **94**, 8016 (1990).
[11] X. Wang, Z. Cao, X. Lu, M. Lin, and Q. Zhang, J. Chem. Phys. **123**, 064315 (2005).
[12] H. Li, X. Kuang, L. Ding, P. Shao, L. Han, and T. Lu, Comput. Mater. Sci. **95**, 600 (2014).
[13] J. van den Brink and G. A. Sawatzky, Europhys. Lett. **50**, 447 (2000).
[14] A. Dolfen, Ph.D. thesis, RWTH Aachen University, 2010.
[15] F. Aryasetiawan, K. Karlsson, O. Jepsen, and U. Schönberger, Phys. Rev. B **74**, 125106 (2006).
[16] T. Miyake, F. Aryasetiawan, and M. Imada, Phys. Rev. B **80**, 155134 (2009).
[17] E. Şaşıoğlu, C. Friedrich, and S. Blügel, Phys. Rev. B **83**, 121101(R) (2011).
[18] T. Kotani, J. Phys.: Condens. Matter **12**, 2413 (2000).
[19] I. Schnell, G. Czycholl, and R. C. Albers, Phys. Rev. B **65**, 075103 (2002).
[20] I. V. Solovyev and M. Imada, Phys. Rev. B **71**, 045103 (2005).
[21] M. Cococcioni and S. de Gironcoli, Phys. Rev. B **71**, 035105 (2005).
[22] F. Aryasetiawan, M. Imada, A. Georges, G. Kotliar, S. Biermann, and A. I. Lichtenstein, Phys. Rev. B **70**, 195104 (2004).
[23] B.-C. Shih, Y. Zhang, W. Zhang, and P. Zhang, Phys. Rev. B **85**, 045132 (2012).

[24] H. Sims, W. H. Butler, M. Richter, K. Koepernik, E. Şaşıoğlu, C. Friedrich, and S. Blügel, Phys. Rev. B **86**, 174422 (2012).
[25] www.flapw.de.
[26] J. P. Perdew, K. Burke, and M. Ernzerhof, Phys. Rev. Lett. **77**, 3865 (1996).
[27] Atomistix ToolKit version 2017, QuantumWise A/S (www.quantumwise.com).
[28] D. Stradi, U. Martinez, A. Blom, M. Brandbyge, and K. Stokbro, Phys. Rev. B **93**, 155302 (2016).
[29] M. Schlipf and F. Gygi, Comput. Phys. Commun. **196**, 36 (2015).
[30] C. Friedrich, S. Blügel, and A. Schindlmayr, Phys. Rev. B **81**, 125102 (2010).
[31] A. A. Mostofi, J. R. Yates, Y.-S. Lee, I. Souza, D. Vanderbilt, and N. Marzari, Comput. Phys. Commun. **178**, 685 (2008).
[32] F. Freimuth, Y. Mokrousov, D. Wortmann, S. Heinze, and S. Blügel, Phys. Rev. B **78**, 035120 (2008).
[33] http://ctcp.massey.ac.nz/dipole-polarizabilities (visited July 2017).
[34] J. Deslippe, M. Dipoppa, D. Prendergast, M. V. O. Moutinho, R. B. Capaz, and S. G. Louie, Nano Lett. **9**, 1330 (2009).
[35] Y. Nomura, M. Kaltak, K. Nakamura, C. Taranto, S. Sakai, A. Toschi, R. Arita, K. Held, G. Kresse, and M. Imada, Phys. Rev. B **86**, 085117 (2012).
[36] A. R. Jani, N. E. Brener, and J. Callaway, Phys. Rev. B **38**, 9425 (1988).
[37] R. Bauer, A. Schmid, P. Pavone, and D. Strauch, Phys. Rev. B **57**, 11276 (1998).
[38] L. Koči, Y. Ma, A. R. Oganov, P. Souvatzis, and R. Ahuja, Phys. Rev. B **77**, 214101 (2008).
[39] G. Kotliar, S. Y. Savrasov, K. Haule, V. S. Oudovenko, O. Parcollet, and C. A. Marianetti, Rev. Mod. Phys. **78**, 865 (2006).
[40] M. W. Haverkort, M. Zwierzycki, and O. K. Andersen, Phys. Rev. B **85**, 165113 (2012).
[41] J. P. Perdew, *Electronic Structure of Solids* (Akademie, Berlin, 1991).